PARTICLE ACCELERATION AT INTERPLANETARY SHOCKS

G.P. ZANK, Gang LI, and Olga VERKHOGLYADOVA
Institute of Geophysics and Planetary Physics (IGPP), University of California, Riverside, CA 92521, U.S.A. (zank@ucr.edu, gang.li@ucr.edu, olgav@ucr.edu)

Received ; accepted

Abstract.
Proton acceleration at interplanetary shocks is reviewed briefly. Understanding this is of importance to describe the acceleration of heavy ions at interplanetary shocks since wave excitation, and hence particle scattering, at oblique shocks is controlled by the protons and not the heavy ions. Heavy ions behave as test particles and their acceleration characteristics are controlled by the properties of proton excited turbulence. As a result, the resonance condition for heavy ions introduces distinctly different signatures in abundance, spectra, and intensity profiles, depending on ion mass and charge. Self-consistent models of heavy ion acceleration and the resulting fractionation are discussed. This includes discussion of the injection problem and the acceleration characteristics of quasi-parallel and quasi-perpendicular shocks.

Keywords: Solar energetic particles, coronal mass ejections, particle acceleration

1. Introduction

Understanding the problem of particle acceleration at interplanetary shocks is assuming increasing importance, especially in the context of understanding the space environment. The basic physics is thought to have been established in the late 1970s and 1980s with the seminal papers of Axford et al. (1977); Bell, (1978a,b), but detailed interplanetary observations are not easily interpreted in terms of the simple original models of particle acceleration at shock waves. Three fundamental aspects make the interplanetary problem more complicated than the typical astrophysical problem: the time dependence of the acceleration and the solar wind background; the geometry of the shock; and the long mean free path for particle transport away from the shock. Consequently, the shock itself introduces a multiplicity of time scales, ranging from shock propagation time scales to particle acceleration time scales at parallel and perpendicular shocks, and many of these time scales feed into other time scales (such as determining maximum particle energy scalings, and escape time scales).

Solar energetic particle (SEP) events are historically classified into two classes "impulsive" and "gradual." Historically, flares have been thought to be the sites of both impulsive and gradual SEPs. A clear association of coronal mass ejections (CMEs) with observed gradual SEP events was

not made until Kahler et al. [1984], who found that large SEPs and CMEs were very highly correlated, as were SEP intensities and the size and speed of the CME. Some earlier charge state measurements [Luhn et al., 1984, 1987; Leske et al., 1995; Mason et al., 1995; Tylka et al., 1995; Oetliker et al., 1997] of energetic ions in gradual SEP events also suggested that these ions originated in regions having $T \simeq 2 \times 10^6$ K, corresponding to coronal material, rather than at a much higher temperature ($T \simeq 2 \times 10^7$ K) flare site. However, puzzling observations, especially after the launch of the ACE spacecraft in the past decade, suggest that high-energy (above tens of MeV) and low-energy particles may result from different seed and acceleration mechanisms dominating different energy regimes [Mason et al., 1999]. Using observations from ACE, Cohen et al. [1999] and Cliver and Cane [2000] present examples of large SEP events associated with impulsive soft X-ray events. These SEP events also had some characteristics of impulsive events, such as high Fe/O ratios. More recently, Cane et al. [2003] studied 29 intense SEP events and found that there are four mixed events which possess both flare and shock accelerated characteristics. Cane et al. [2003] considered 30 - 50 Mev/nuc. energies in Fe and O. These events usually have a time intensity profile that looks like those due to shock acceleration but have a flare-like composition. It is possible that these are the events in which CMEs and the accompanying flares occur temporally close to each other and are both well connected magnetically to the Earth. For such cases, some of the solar flare material will undergo shock reacceleration (see Li and Zank [2005]) and thus have a time intensity profile similar to shock accelerated particles.

To better understand in situ measurements (time-intensity profiles, particle spectra, relative heavy ion abundances, etc.) of gradual SEP events and to help clarify the ambiguous relationship between flares and CMEs, a detailed model of ion acceleration and transport at CME-driven shocks is necessary. Earlier works by Heras et al. [1992, 1995], Ruffolo [1995], Kallenrode and Wibberenz [1997], Kallenrode and Hatzky [1999], Lario et al. [1998], and Ng et al. [1999, 2003] adopted a "black-box" approach to particle acceleration at propagating CME-driven shocks, simply injecting ion spectra at the shock, thus neglecting all the physics of diffusive shock acceleration, and focussed on the transport of energetic particles in the interplanetary medium by solving the Boltzmann-Vlasov equation numerically. Ng et al. [2003] has extended his earlier models [Ng et al., 1995, 1999], by allowing energetic particles and the generated Alfven waves to interact self-consistently. The amplification of the Alfven waves is determined by the particle anisotropy. Particles escaping from the shock at earlier times generate the necessary waves for accelerating particles at a later time. Non-trivial SEP time intensity profiles can result [Ng et al., 2003]. While the Ng et al. [2003] approach marked a significant step toward a better understanding of gradual SEP events, it assumed a prescribed particle spectrum (power law at low energies and an exponential

rollover at high energies) at a CME shock propagating at a constant speed with an assumed radial magnetic field. This approach therefore neglects much of the basic physics of time-dependent diffusive particle acceleration. Furthermore, the assumption that the shock propagates at a constant speed in the solar wind is clearly not reasonable.

Li et al. [2005] presented a model which calculates the acceleration of heavy ions at a CME-driven or an interplanetary shock wave and their subsequent transport in the interplanetary medium. This work is based on a series of papers by Zank et al. [2000], Rice et al. [2003], and Li et al. [2003]. These models assume particle acceleration at a quasi-parallel shock. The extension of these ideas to quasi-perpendicular shocks has been presented in Zank et al. (2006). The basic physics underlying these models is discussed below.

A brief overview of shock acceleration at quasi-parallel and quasi-perpendicular shocks will be given, including our approach to particle transport in the interplanetary medium. These ideas will be applied to the acceleration of heavy ions at interplanetary shocks, and we will conclude by modelling some real SEP and ESP events.

2. Particle acceleration models and transport

2.1. Acceleration at quasi-parallel shocks

Zank et al. [2000] model the evolution of a CME-driven shock wave. At the shock front, the accelerated particle spectrum is produced by diffusive shock acceleration. For diffusive shock acceleration to be applicable, magnetic turbulence near the shock is necessary to scatter particles repeatedly across the shock. For quasi-parallel shocks, the turbulence (Alfvén waves) is generated by the anisotropic energetic protons at the shock [Bell, 1978a; Lee, 1983]. Furthermore, since the number density of heavy ions is negligible compared with that of protons, the turbulence is due solely to the streaming protons. Heavy ions can therefore be treated as test particles, experiencing the turbulence but not contributing to its generation. We consider two species of heavy ions, viz., CNO particles and iron, with charge $Q = 6$ and mass $A = 14$ corresponding to CNO particles and $Q = 14$ and $A = 56$ corresponding to iron.

The resonance condition for particles and waves is given by the Doppler condition,

$$\omega - \Omega = k_{\|}\mu p/\gamma m, \tag{1}$$

where ω is the resonant wave frequency, Ω is the local ion gyrofrequency, $k_{\|}$ is the wave vector along the magnetic field, μ the particle pitch angle cosine, p the particle momentum, m (m_p) the particle (proton) mass, and

γ the Lorentz factor. Higher order resonances are not considered. The ion gyrofrequency is $\Omega = (Q/A)eB/\gamma m_p c$ (in Gaussian units), where Q is the particle charge, A the ion mass number, and c the speed of light. In the context of particle acceleration of heavy ions at a quasi-parallel shock, the resonant wave number for an ion of mass A and charge Q is

$$k \simeq \frac{Q}{A}\frac{eB}{\tilde{p}c}, \tag{2}$$

where $\tilde{p} = p/A$ denotes particle momentum per nucleon. (See Gordon et al., 1999 and Li et al., 2005 for a discussion of the resonance broadening assumption implicit in (2).) Physically, the Doppler condition means the phase of the Alfvén wave seen by the particle is unchanged after a gyration. The diffusion coefficient for particles in resonance with the Alfvén wave depends on the wave intensity $I(k)$ through

$$\kappa(p) = \frac{vp^2c^2}{8\pi Q^2e^2}\frac{1}{I(k = \Omega/v)}. \tag{3}$$

The wave intensity $I(k,t)$ can be obtained from the wave kinetic equation (Lee, 1983; Gordon et al., 1999; Rice et al., 2003), and depends on the obliquity of the shock, going to zero as the shock becomes increasingly perpendicular. For strong shocks, the wave intensity can be approximated by B^2/k, and the Bohm approximation used in Zank et al. [2000] is recovered.

The propagation of the shock in the solar wind is modelled numerically and the post shock flow is determined completely consistently. We use an MHD model for the shock and solar wind. In the shell model of Zank et al. (2000), the region over which the shock sweeps is approximated by a set of concentric shells. At some time t, the shock is located at $R(t)$. A new shell is then created with the outer edge and inner edge initially coincident with the shock front at $R(t)$. After a time Δt later, the outer edge of the shell, which is attached to the shock, propagates to $R(t + \Delta t)$ whereas the inner edge of the shell propagates to $R(t) + v_{sw}\Delta t$. Thus, the shell is created and will decouple from the shock. After $t + \Delta t$, the shock continues to propagate and convect in the supersonic solar wind according to the self-consistent MHD model, and a new shell is created. Shock properties, such as shock speed and compression ratio, are followed numerically as the shock wave expands. At the shock, the accelerated particle spectrum is obtained by adopting the diffusive shock acceleration solution for a planar shock, subject to the assumption that the time dependent parameters of the shock (i.e. the shock Mach number and compression ratio) can be regarded as locally constant. This leads to,

$$f(t_i,p) = \frac{\beta N}{4\pi p_{inj}^3 u_{up}}\left(p/p_{inj}\right)^{-\beta(t_i)}\{H[p - p_{inj}(t_i)] - H[p - p_{max}(t_i)]\}. \tag{4}$$

Here, $\beta(t_i)$ [$= 3s_i/(s_i - 1)$, s_i the shock compression ratio] is the spectral index of the shock accelerated ions, the variable t_i represents the ith time step in the code, N the injection rate, H the Heaviside step function, u_{up} the upstream flow speed, and p_{inj} and p_{max} are the injection and maximum momentum of the accelerated protons, and correspond to the maximum turbulence wave number $k_{max} = eB/p^p_{inj}c$ and the minimum turbulence wave number $k_{min} = eB/p^p_{max}c$. The superscript p indicates proton. For wave numbers smaller (larger) than the minimum (maximum) wave number, the corresponding wave intensity will be that of the ambient solar wind.

We choose p_{inj} so that $p^2_{inj}/2m_p$ corresponds to the downstream thermal energy per nucleon, and assume that the injection momentum per nucleon is the same for protons and heavy ions, $\tilde{p}^p_{inj} = \tilde{p}^{CNO}_{inj} = \tilde{p}^{Fe}_{inj}$. We therefore assume that at a quasi-parallel shock, the injection mechanism for diffusive shock acceleration does not distinguish protons from heavy ions. Furthermore, because of the weak dependence of $\tilde{p}_{max}$ on $\tilde{p}_{inj}$, we expect this to be a reasonable assumption.

As the interplanetary shock propagates outward, it slows, its strength decreases, and its area increases, and the steady-state solution (4) holds only approximately (and locally). The maximum momentum for protons can be determined by equating the dynamical timescale of the shock and the acceleration time scale [Drury, 1983; Zank et al., 2000],

$$\frac{R(t) - R_0}{\dot{R}(t)} \simeq \frac{\beta(t)}{u^2_{up}} \int_{p_{inj}}^{p_{max}} \kappa(p') d(\ln(p')). \tag{5}$$

In (5), $R(t)$ is the shock speed in the spacecraft frame, R_0 the position of shock formation ($\sim 5R_\odot$). The solution of (5) yields p_{max} for protons, and hence the lower limit of the excited resonant wave number, as [Zank et al., 2000]

$$p_{max} \simeq \left\{ \left[\frac{M^2(t) + 3}{5M^2(t) + 3} \frac{(R(t) - R_0)}{\beta(t)\kappa_0} \frac{B}{B_0} + \sqrt{\left(\frac{m_p c}{p_0}\right)^2 + \left(\frac{p_{inj}}{p_0}\right)^2} \right]^2 - \left(\frac{m_p c}{p_0}\right)^2 \right\}^{1/2}. \tag{6}$$

Expression (6) illustrates explicitly that the maximum energy to which a particle can be accelerated depends on the age of the shock $R(t)$, the strength of the shock $\dot{R}(t)$, and the interplanetary magnetic field strength B. Heavy ions experience only the turbulence generated by the streaming protons. Thus the maximum achievable momentum for heavy ions is subject to the constraint (2), which shows that the maximum heavy ion momentum $\tilde{p}^i_{max}$ and the maximum proton momentum $\tilde{p}^p_{max}$ are related through the minimum turbulence wave number k_{min} by

$$\frac{eB}{\tilde{p}^p c} = k_{min} = \frac{Q^i}{A^i} \frac{eB}{\tilde{p}^i c}, \tag{7}$$

and i indicates either CNO or Fe particles. The (A/Q) dependence of $\tilde{p}$ is evident. Illustrated in Figure 1 are the maximum particle energies for protons, O, and Fe ions as a function of radial distance. In most of the plots that follow, we will use the results of Verkhoglyadova et al. (2007) who have modelled several observed gradual SEP events on the basis of the theory described here.

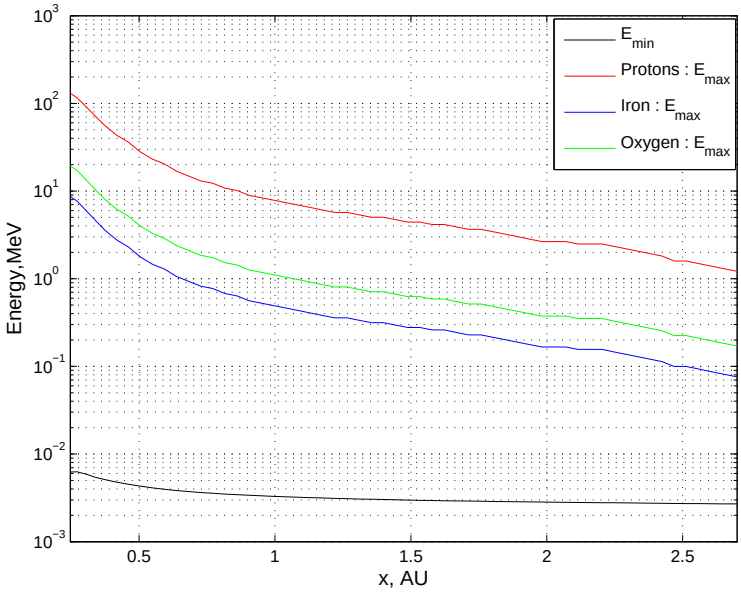

Figure 1. Plot of the maximum and minimum proton, O, and Fe energies per nucleon as a function of heliocentric distance for the September 29, 2001 SEP event. Note that the ordering of maximum energies is inversely dependent on particle mass, and that the maximum energy decreases with distance i.e., both $\dot{R}(t)$ and B compensate for $R(t)$. Verkhoglyadova et al. (2007).

Downstream of the shock, energetic particles convect with the solar wind, adiabatically cool, and diffuse. The shell model allows us to follow the evolution of the particle phase space distribution function f downstream of the shock quite straightforwardly. The convection, adiabatic cooling, and diffusion of particles are treated using an operator splitting technique. First, the convection of particles with the solar wind is followed by updating the locations of the front and back boundaries of each shell after each time step. As the shell convects outward, it also expands radially. From Liouvilles theorem, the radial expansion leads to a cooling in p space. Finally, particles can diffuse to adjacent shells depending on their diffusion coefficient, and also leak out from the shock complex if during time step they reach some distance $l(r, p, t)$ in front of the shock (see Li et al., 2005).

2.2. Quasi-perpendicular shocks

While the theory of particle acceleration at a quasi-parallel shock appears to be reasonably well understood, no similar theory exists for perpendicular shocks. Zank et al. (2006) developed an approach for diffusive shock acceleration at perpendicular shocks. Particle acceleration via the first-order Fermi mechanism at a perpendicular shock wave remains an outstanding problem for two essential reasons. The first is that, unlike the quasi-parallel shocks discussed above, accelerated particles at a perpendicular shock cannot excite the [Alfvén] wave field that is responsible for scattering the particles repeatedly across the shock. This is because the growth term in the wave equation is proportional to $\cos\theta_{bn}$, where θ_{bn} is the angle between the upstream magnetic field and the shock normal direction, and is thus 90° for a strictly perpendicular shock (e.g., Gordon et al., 1999; Li et al., 2003; Rice et al., 2003). Unlike the particle acceleration model described in 2.1, this therefore requires that particle scattering at a perpendicular shock be the result of in situ upstream turbulence that is convected into the shock. At the heart of the problem for perpendicular shocks is the need for a viable model of the perpendicular component of the diffusion tensor. The second problem is that since an accelerated particle is essentially tied to a magnetic field line, its ability to cross the shock repeatedly is limited to the time it takes a magnetic field line to cross from upstream to downstream, assuming that the magnetic field line experiences some wandering to make the transmission time non-zero. Thus, a fast moving particle is necessary if it is to experience multiple crossings of the perpendicular shock (see Figure 2) so that it can be diffusively accelerated. Consequently, diffusive shock acceleration of particles at a perpendicular shock is effective for particles that are already energetic. This is referred to as the "injection problem" for perpendicular shocks [Jokipii, 1987; Zank et al., 1996].

It is generally thought that the acceleration time at a quasi-parallel shock is much larger than that at a quasi-perpendicular shock. This result is however predicated on the assumption that the intensity of the upstream turbulence is the same at a parallel and perpendicular shock, which, as we have seen above, is incorrect because waves are excited at a quasi-parallel shock and not at a quasi-perpendicular shock. A physically meaningful comparison of acceleration time scales must take this into account.

On the basis of a recently developed nonlinear guiding center theory for the perpendicular spatial diffusion coefficient $\kappa_\perp$ used to describe the transport of energetic particles (Matthaeus et al., 2003; Zank et al., 2004), Zank et al. (2006) constructed a model for diffusive particle acceleration at highly perpendicular shocks i.e., shocks whose upstream magnetic field is almost orthogonal to the shock normal. They use $\kappa_\perp$ to investigate energetic particle anisotropy and injection energy at shocks of all obliquities, finding

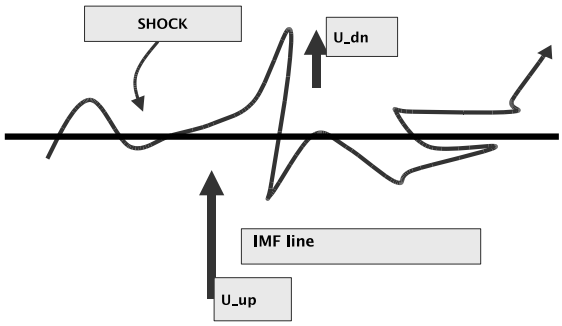

Figure 2. Schematic showing an interplanetary magnetic field (IMF) line experiencing random walking as it is convected through a shock. A particle attached to the field line can make multiple excursions up- and downstream as the field line is carried completely through the shock, provided the particle is moving sufficiently fast. This requires that particles already be energetic if they are to experience diffusive shock acceleration at a perpendicular shock. U_{up} and U_{dn} refer to the upstream and downstream flow speeds. Zank et al. (2006)

that at 1 AU, for example, parallel and perfectly perpendicular shocks (i.e., the shock normal is exactly 90° to the upstream magnetic field) can inject protons with equal facility. However, at highly oblique shocks, high injection energies are necessary, as is illustrated in Figure 3. As discussed by Zank et al. (2006), since interplanetary shocks are typically highly oblique (rather than perfectly perpendicular), injection is likely to be sporadic, suggesting, as found by van Nes et al. (1984), that the low-energy event intensity decreases as a shock becomes more perpendicular.

An important point not hitherto recognized is that the inclusion of self-consistent wave excitation at quasi-parallel shocks in evaluating the particle acceleration timescale ensures that it is significantly smaller than that for highly perpendicular shocks at low to intermediate energies and comparable at high energies. Thus, higher proton energies are achieved at quasi-parallel rather than highly perpendicular interplanetary shocks within 1 AU. However, both injection energy and the acceleration timescale at highly perpendicular shocks are sensitive to assumptions about the ratio of the 2D correlation length scale λ_{2D} to the slab correlation length scale λ_{slab} (Figure 3).

By adapting the approach developed in Zank et al. [2000] and Li et al. [2003], Zank et al. (2006) have developed a model for particle acceleration at a perpendicular interplanetary shock. Just as at a quasi-parallel shock, the usual stationary cosmic ray transport equation can be solved at a perpendicular shock, yielding the same spectral dependence on the shock compression ratio in both cases. The differences between the two cases are the scaling of the upstream exponential decay of particle intensity, the injection energy,

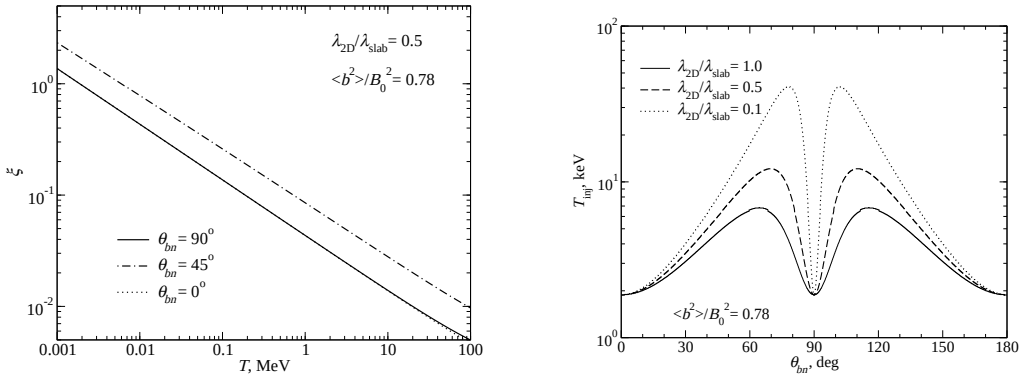

Figure 3. Left: A plot of the anisotropy ξ ahead of a shock as a function of energy for parallel, oblique, and perpendicular shocks. A compression ratio of $s = 3$ is assumed. Note that at low energies, the perpendicular and parallel shocks have almost identical values of ξ. Right: Plot of the injection energy as a function of the shock obliquity under the assumption that $\xi = 1$ defines the threshold energy for injecting particles into the diffusive shock acceleration mechanism. Three possible ratios of $\lambda_{2D}/\lambda_{slab}$ are considered. In both the left and right panels, parameters corresponding to an interplanetary shock located at 1 AU are used. Note that the $\theta_{Bn} = 0°$ curve is almost completely obscured by the $\theta_{Bn} = 90°$ curve. Zank et al. (2006)

and the maximum energy, since all of these depend on the spatial diffusion coefficient.

As discussed above, the local injection momentum or velocity for particles to be accelerated diffusively at highly oblique shocks is much more stringent than at quasi-parallel shocks, and is given by (Zank et al., 2006)

$$v_{inj} = 3u \left[\frac{1}{(s-1)^2} + \frac{r_L^2 + \lambda_\parallel^2 \cos^2\theta_{bn}}{\left(\lambda_\perp + \lambda_\parallel \cos^2\theta_{bn}\right)^2} \right]^{1/2}, \tag{8}$$

As with the quasi-parallel case, a similar approach, but using now the NLGC model for the perpendicular diffusion coefficient, can be followed to estimate the maximum particle momentum p_{max}. This is now very complicated analytically within the NLGC framework, and Zank et al. (2006) solve the corresponding integro-differential equation numerically. However, estimates for p_{max} can be determined for shocks within several AU, i.e., for shock accelerated particles with gyroradii that exceed the correlation length scale. For arbitrary mass and charge ions, Zank et al. (2006) compute the maximum particle momentum as

$$\tilde{p}_{max} \simeq \left(\frac{Q}{A}\right)^{2/3} \left(\frac{e}{m_p}\right)^{2/3} \frac{R}{\dot{R}} \frac{(s-1)}{s} \frac{V_{sh}^2}{1.17\alpha} \lambda_c^{slab} \langle b_{slab}^2 \rangle, \tag{9}$$

where $\tilde{p}$ is the momentum per nucleon, and $\langle b^2_{slab} \rangle$ is the energy density of magnetic field fluctuations. The dimensional constant α has units $\mathrm{cm}^{4/3}\mathrm{s}^{-2/3}$ (see Zank et al., 2006). The maximum momentum expression reveals several interesting points. A fundamental difference between the perpendicular and quasi-parallel expressions is that the former assumes only pre-existing turbulence in the solar wind, whereas the latter results from solving the coupled wave energy and cosmic ray streaming equation explicitly, i.e., in the perpendicular case, the energy density in slab turbulence corresponds to that in the ambient solar wind whereas in the case of quasi-parallel shocks, it is determined instead by the self-consistent excitation of waves by the accelerated particles themselves. From another perspective, unlike the quasi-parallel case, the resonance condition does not enter into the evaluation of p_{max} given in (9). As a result, the diffusion coefficient is fundamentally different in each case, and hence the maximum attainable energy is different for a parallel or perpendicular shock.

Some comments regarding the determination of p_{max} for different shock configurations and ionic species are useful since three approaches have been identified [Zank et al., 2000; Li et al., 2003; Zank et al., 2006]. 1. For protons accelerated at a quasi-parallel shock, p_{max} is determined purely on the basis of balancing the particle acceleration time resulting from resonant scattering with the dynamical timescale of the shock. The wave/turbulence spectrum excited by the streaming energized protons extends in wave number as far as the available dynamical time allows. 2. For heavy ions at a quasi-parallel shock, the maximum energy is also computed on the basis of a resonance condition but only up to the minimum k excited by the energetic streaming protons, which control the development of the wave spectrum. Thus, maximum energies for heavy ions are controlled by the accelerated protons and their self-excited wave spectrum. This implies a $(Q/A)^2$ dependence of the maximum attainable particle energy for heavy ions. 3. For protons at a highly perpendicular shock, the maximum energy is independent of the resonance condition, depending only on the shock parameters and upstream turbulence levels. For heavy ions, this implies either a $(Q/A)^{1/2}$ or a $(Q/A)^{4/3}$ dependence of the maximum attainable particle energy, depending on the relationship of the maximum energy particle gyroradius compared to the turbulence correlation length scale. The summary presented here suggests that it may be possible to extract observational signatures related to the mass - charge ratio that distinguish particle acceleration at quasi-parallel and highly perpendicular shocks.

Zank et al. (2006) consider a CME-driven shock propagating from 0.1 AU to ~ 1 AU, making the somewhat simplistic assumption that the shock remains either parallel or that $\theta_{bn} = 85^\circ$. The dependence of injection energy and the maximum energy to which a particle can be accelerated as a function of radial distance is illustrated in Figure 4 for a perpendicular

shock. The figure compares the corresponding energies for an otherwise identical parallel shock where the energetic particles excite the upstream wave spectrum (a subtlety that has been neglected in previous comparisons of particle acceleration at perpendicular and parallel shocks), assuming that the shock remains parallel for the duration of its propagation to 1 AU. Since we assume wave excitation in the parallel shock calculation, this results in maximum energies that can be as much as an order of magnitude larger at a parallel shock than at a perpendicular shock close to the sun. The maximum energies accelerated at parallel and perpendicular shocks begin to converge towards 1 AU. The decay in maximum energy is slower for the perpendicular shock than the parallel because of the slower WKB-like decrease in energy in turbulent fluctuations and because of the $1/r^2$ dependence of B within 1 AU for the parallel case. We stress that in the absence of the self-consistent wave excitation, the perpendicular shock would accelerate particles to higher energies than a parallel shock.

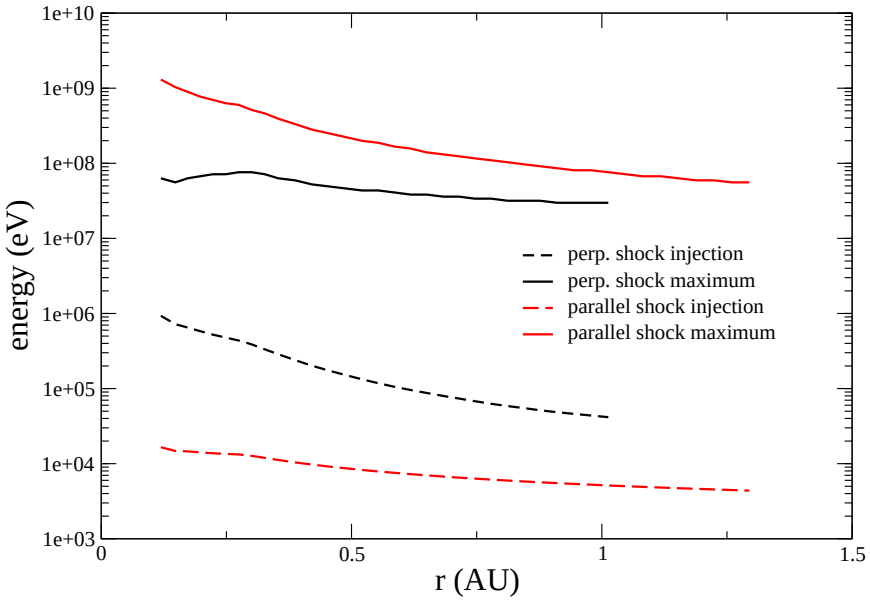

Figure 4. Maximum particle energy and injection energy for a highly perpendicular shock (85°, black curves) as a function of heliocentric distance. For comparison, we plot the corresponding results for a parallel shock (red curves). Zank et al. (2006)

2.3. Particle transport in the interplanetary medium

The Boltzmann-Vlasov equation describes the evolution of the distribution function $f(r, p, t)$ for energetic particles escaping from the shock front into

the interplanetary medium,

$$\frac{\partial f}{\partial t} + \frac{p}{m} \cdot \nabla f + \mathbf{F} \cdot \nabla_p f = \frac{\partial f}{\partial t}\Big)_{coll}, \tag{10}$$

where the right hand side describes particle collisions; in this case, the scattering of charged particle by fluctuations in the IMF. Ignoring the collision term, the characteristics of the Boltzmann equation are simply the equations of motion for a single particle. Thus, solving the Boltzmann equation can be achieved by following individual particle motion, which consists of an interplay between collisionless motion and occasional pitch angle scattering. A Monte-Carlo code was developed by Li et al. (2003) to follow charged particle motion in the IMF. The frequency of scattering can be parameterized by the mean free path $\lambda_{\|}$. Following Zank et al. [1998] and Li et al. [2003, 2005], we may express the particle mean free path as

$$\lambda_{\|} = \lambda_0 \left(\frac{\tilde{p}c}{1\mathrm{GeV}}\right)^{1/3} \left(\frac{A}{Q}\right)^{1/3} \left(\frac{r}{1\mathrm{AU}}\right)^{2/3}, \tag{11}$$

where λ_0 is a normalizing mfp (typically 0.1 - 1 AU, from observations). Note the presence of an $(A/Q)^{1/3}$ dependence in equation (11). For Fe and CNO particles with the same momentum per nucleon $\tilde{p}$, Fe will have a larger mean free path than CNO particles because of the larger A/Q ratio.

Between consecutive pitch angle scatterings, charged particles gyrate along the IMF. As the magnetic field expands radially, particles experience adiabatic cooling and focusing effects as a consequence of adiabatic invariants of the motion. The geometry of the magnetic field B is given by the usual Parker spiral [Parker, 1958],

$$B = B_0 \left(\frac{R_0}{r}\right)^2 \left[1 + \left(\frac{\Omega_0 R_0}{u}\right)\left(\frac{r}{R_0} - 1\right)^2 sin^2\theta\right]^{1/2} \tag{12}$$

where θ is the colatitude of the solar wind with respect to the solar rotation axis; Ω_0 the solar rotation rate; u the radial solar wind speed, and B_0 the interplanetary magnetic field (IMF) at the corotation radius R_0 (typically, $R_0 = 10R_\odot$, $B_0 = 1.83 \times 10^{-6}$ T, $u = 400$ km/s, and $\Omega_0 = 2\pi/25.4$ days).

After the initial condition (t, p) of a test particle escaping from the shock complex is decided, Li et al. (2003, 2005) then follow its subsequent motion, i.e., "free" motion and pitch angle scattering until the shock passes 1 AU. The scattering is assumed to be isotropic and Markovian; thus the new pitch angle after a scattering has no memory of the previous pitch angle. Since the shock is expanding outward, particles are subject to possible "absorptions" by the shock before it reaches 1 AU. This could happen, for example, if a particle is moving inward towards the sun due to pitch angle scattering or

if the particle speed along the magnetic field is so small that the shock can catch it from behind. Once a particle is absorbed, it can be re-accelerated if its energy is smaller than the current maximum energy associated with the shock. The code contains adiabatic cooling, focussing, and mirroring - see Li et al. [2003] for details.

3. Modelling observed events

3.1. Differences between particle acceleration at perpendicular and parallel shocks

The differences in particle injection and maximum particle momenta between quasi-parallel and perpendicular shocks were illustrated in Figure 4. In Figure 5, we show the evolution of the accelerated energetic particle relative number density at 1 AU as a function of time for the example of a quasi-perpendicular and parallel shock. The solid curves correspond to the quasi-perpendicular shock $\theta_{bn} = 85^\circ$ and the dotted curves to the parallel shock accelerated protons. The total number of injected particles in the parallel shock case is assumed to be 20 times greater than that of the perpendicular shock. This ratio is in agreement with results obtained by *Mewaldt et al.* [2001] - see Zank et al. (2006). Since the Zank et al. (2006) model is crude, they did not follow the time evolution of injected particles at a perpendicular shock, but instead assumed that the total number of injected particles at the quasi-perpendicular shock remains 20 times smaller than that at the parallel shock.

At early times, the quasi-perpendicular shock has a much clearer power law extending from lower energies than the parallel case. This is a consequence of quasi-perpendicular shocks not being as effective at trapping particles at the shock front as parallel shocks, which ensures that relatively more particles escape at lower energies from the highly perpendicular shock than at the parallel shock. Consequently, a power law spectrum is more likely to be seen at earlier times. The parallel shock can accelerate particles to higher energies and this is revealed clearly in Figure 5. The parallel shock spectra tend to fill out into a power law over time until at 1 AU it almost resembles the perpendicular shock example, except that it is shifted out to higher energies.

Shown in Figure 6 are the corresponding intensity profiles for a quasi-perpendicular (top panel) and parallel (bottom panel) shock. Three energies are illustrated. Clear differences between the two models are evident. Thanks to wave excitation by the streaming instability at the parallel shock, the parallel diffusion coefficient is smaller at these energies than the diffusion coefficient at the quasi-perpendicular shock. Consequently, particle trapping

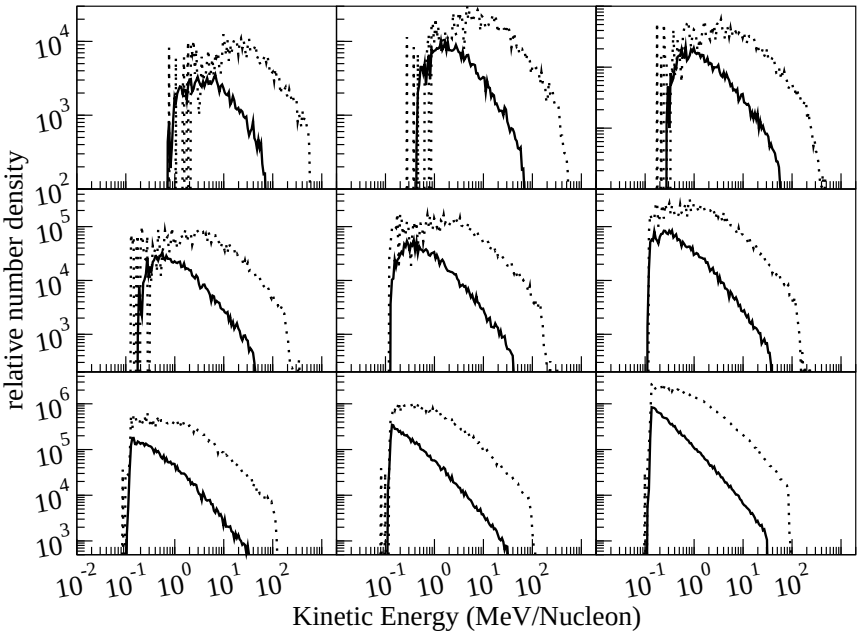

Figure 5. The time interval spectra for a perpendicular (solid line) and a parallel shock (dotted line). From left to right and top to bottom, the panels correspond to the time intervals $t = (1 - 8/9)T$, $t = (1 - 7/9)T, \cdots, t = (1 - 1/9)T$, where T is the time taken for the shock to reach 1 AU. Note particularly the hardening of the spectrum with increasing time for the perpendicular shock example. Zank et al. (2006)

is more efficient at the parallel shock, thus limiting particle escape at the energies illustrated. This is reflected in the intensity profiles, which show a very rapid rise time and formation of a plateau in the quasi-perpendicular shock case. A much slower rise time is exhibited in the parallel shock example and only the $T = 50$ MeV protons reach a plateau phase (by contrast, the 50 MeV particles accelerated at the quasi-perpendicular shock are released rapidly enough that they are no longer observed at 1 AU after ~ 1 day). Like the spectra illustrated in Figure 5, distinctive differences are present in the intensity profiles associated with quasi-perpendicular and parallel shocks. These will of course not be revealed as clearly in observations as they are in our models since we have deliberately neglected the changing obliquity of the shock with heliocentric radius and the spacecraft connection to different magnetic field lines with time.

3.2. Modelling a quasi-parallel event

The theory discussed above in 2.1, 2.2, 2.3 is now becoming reasonably well established, but very few attempts have been made to model directly particle acceleration and transport of specific events (see e.g. Li et al., 2005, Tylka

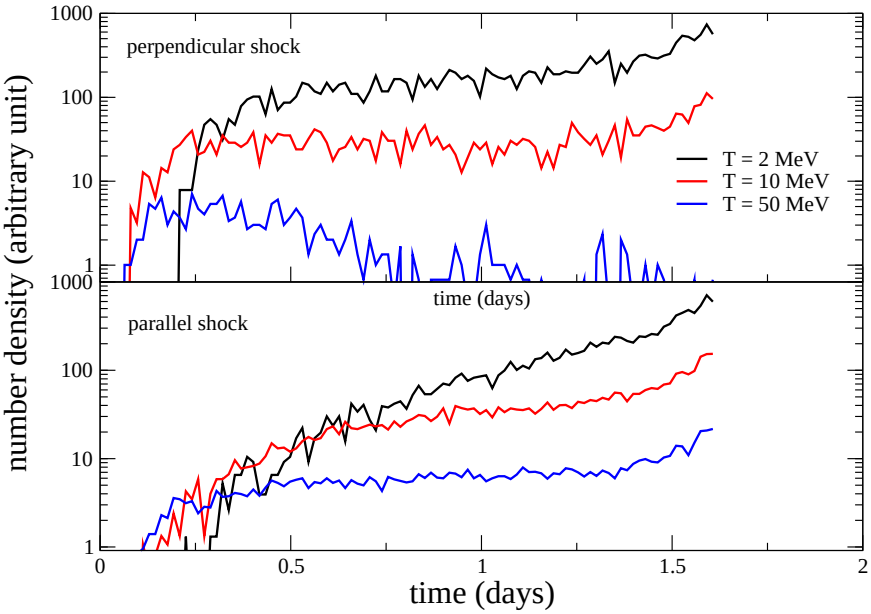

Figure 6. Time intensity profiles for the quasi-perpendicular and parallel shock cases. The upper panel is for the perpendicular shock case and the lower for the parallel shock case. The shock arrived at 1 AU about 1.6 days after initiation. The basic details of the model and the related physics are discussed in *Zank et al.* [2000], *Li et al.* [2003], and *Rice et al.* [2003]. The intensity profiles emphasize the important role of the time dependent maximum energy to which protons are accelerated at a shock and the subsequent efficiency of trapping these particles in the vicinity of the shock. Compared to the parallel shock case, the particle intensity reaches the plateau phase faster for the quasi-perpendicular shock example. This is because $\kappa_\perp$ at a highly perpendicular shock is larger than the stimulated $\kappa_\parallel$ at a parallel shock, so particles (especially at low energies) find it easier to escape from the quasi-perpendicular shock than the parallel shock. Zank et al. (2006)

et al., 2005). In part, this is due to 1) the difficulty in modelling the physical conditions pertaining to the initial conditions in the solar wind, including shock initiation, formation, and location; the initial shock speed, obliquity, upstream solar wind plasma conditions; the pre-turbulence levels at the shock; the ambient seed population, etc., and 2) the magnetic connection of the spacecraft to the propagating shock varies temporally.

To address the second problem, a fully 2-D model is needed. In particular, the model should include a treatment of particle acceleration at perpendicular shocks similar to that outlined in section 2.2. While a 2-D model is important and perhaps necessary to understand most SEP events, a model that focuses on quasi-parallel shocks can nevertheless still provide a reasonable description of some SEP events. Needless to say, these events are not common, since they must maintain a quasi-parallel configuration during their propagation from the Sun to 1 AU. In this section, we discuss a very

detailed modelling effort by Verkhoglyadova et al. (2007) for a particular quasi-parallel event.

As a first step, Verkhoglyadova et al. (2007) identified 7 quasi-parallel shocks at 1 AU from the ACE List of Disturbances and Transients (maintained by C.W. Smith) and the MIT shock database (maintained by J. Kasper). Of course, these shocks may not have been quasi-parallel near the Sun, in which case we expect that our 1D model simulation and the observations may differ, especially in the early time intensity profiles. In view of the distinctions between quasi-parallel and quasi-perpendicular shock time intensity profiles and the dependence of the break point on (Q/A), we can expect that if the observed time intensity profiles and the modeled calculation agree reasonably well, then the shock being modeled was quasi-parallel throughout its propagation. More accurately, the shock associated with the connection point of the interplanetary magnetic field and the spacecraft as the shock traversed the interplanetary medium to 1 AU remained in a quasi-parallel configuration. Were this the case, we can further examine the (Q/A) dependence of the break point of the energy spectra for heavy ions to better support our assumption of quasi-parallel shock propagation from the sun to 1 AU.

Having identified a potentially suitable quasi-parallel shock, we next determine if SEP signatures at 1AU can be associated with it. This step of the analysis is frequently complicated by the possibility that an observed SEP event at 1 AU may often be the result of particle acceleration at and/or interaction with two or more CME shocks. Ideally, the identification of "clean" SEP events with pre-event backgrounds that are clearly free of "contamination" from earlier (small or large) SEP events or even previous impulsive events is preferred. However, besides the difficulty in identifying such infrequent events, a persuasive argument can be made that such "stirred up" conditions are conducive to particle acceleration at interplanetary shocks (enhanced levels of both pre-energized particles - for injection - and low-frequency magnetic turbulence - for particle scattering). Consequently, we do not impose the requirement that a clean pre-event background is necessary when selecting an event. Instead, a quasi-parallel shock is included in our study if careful examination of particle spectra and time intensity suggests the possibility of diffusive shock acceleration.

The numerical model of 2.1 and 2.3 developed at the IGPP, University of California at Riverside is called the **P**article **A**cceleration and **T**ransport in the **H**eliosphere model (hereafter PATH). The model consists of two major parts. The first part includes modelling of an evolving shock and particle acceleration, and the second one treats energetic particle transport throughout the heliosphere (from 0.1 to $>$ 1 AU). The core of the PATH model is described in Zank et al., 2000; Rice et al., 2003; and Li et al., 2003, 2005. As described in 2.1, the spatial diffusion coefficient for the quasi-

parallel shock is calculated self-consistently (Gordon et al., 1999; Rice et al., 2003). The injection momentum is a parameter that can be adjusted, and is currently taken as ~ 10 keV.

After verifying the appropriate SEP signatures at 1 AU, we then numerically model the solar wind background and shock, tuning the model to yield as accurately as possible the pre-event conditions. This includes using real-time solar wind parameters prior to the event as the background input and adjusting the initial CME-driven shock speed, density and temperature jumps at the inner boundary to obtain results that closely mimic the observed shock speed and compression ratio at 1 AU. After obtaining a realistic solar wind, the PATH model then follows the shock evolution, the associated particle acceleration, and finally the transport of accelerated energetic particles throughout the heliosphere(from ~ 0.1 to beyond 1 AU).

A case identified by Verkhoglyadova et al. (2007) as an appropriate candidate to model was an event that occurred on September 29, 2001. From the MIT shock database maintained by J. Kasper, the average angle between the shock normal and the background magnetic field is estimated as $\sim 19^\circ$ (another estimate gives 25.7°) which justifies the approximation of a quasi-parallel shock. The shock reached 1 AU with a speed of ~ 700 km/sec at 9:10 on 29 September 2001. The compression ratio was $s \sim 2.3$. Prior to the arrival of the shock, a partial halo CME with a speed of 1109 km/s was observed by SOHO/LASCO at 04:54:05 on 27 September 2001 (from the LASCO CME catalogue). From 04:32 to 04:38 on 27 September 2001, x-rays were also observed in the active region 9628, located at S20W27, by GOES.

As documented by Desai et al., 2003, there is a large SEP event on September 24, 2001. The example that Verkhoglyadova et al. (2007) consider occurs during the decay phase of this large SEP event. A careful examination of the Fe time intensity profile, for example, shows quite convincingly that particle acceleration occurred at the September 29, 2001 shock. In Figure 7, we show plots at various energies of the Fe time intensity profile using ULEIS and SIS energies. At energies drawn from ULEIS (Figure 7 (left panel)), a local bump in the time intensity is clearly seen close to $t = 60$ hours (with 0 starting from day 270) when the September 29, 2001 shock arrived, a clear signature of diffusive shock acceleration. At higher SIS energies (Figure 7 (right panel)), although the gradually decaying background from the previous event is high, we can still infer particle acceleration associated with the September 29, 2001 event through, for example, the increase in the $E = 19.3$ MeV/nucleon profile. Between $t = 10 - 35$ hours (from day 270), there is a relatively abrupt enhancement over the background followed by an equally abrupt decrease. As we discuss below, we may anticipate that this enhancement is associated with the early acceleration of Fe ions by the September 29 shock for a short period. (It is possible that the time intensity

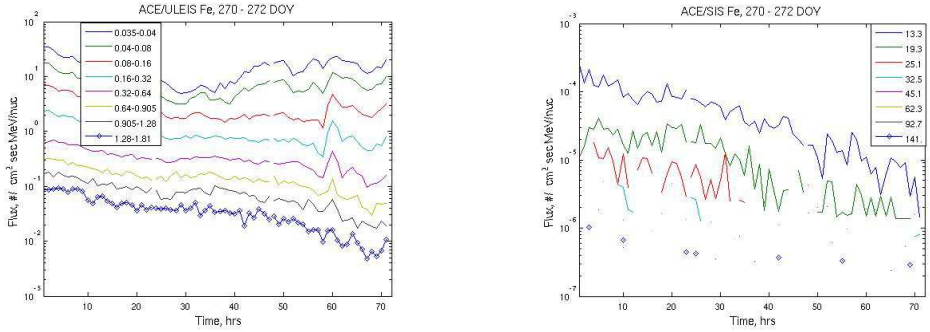

Figure 7. Time intensity profiles drawn from ACE ULEIS (left) and SIS data (right) at a range of energies, given in MeV/nucleon. Verkhoglyadova et al. (2007)

profiles of these two events could be separated using a detailed simulation that includes both shocks. This is left for future work.)

As suggested earlier, a prior shock primes the interplanetary medium by seeding it with energetic particles that the second shock can inject and (re)accelerate. Diffusive shock acceleration may well therefore be easier or more efficient for a shock that follows another. A careful injection model for pre-existing energetic particles should include their spectral form, abundances, etc. but for the present, Verkhoglyadova et al. (2007) assumed that these particles are simply assimilated and reaccelerated at the second shock. This is reasonable since the reacceleration of a pre-existing spectrum produces a new spectrum with characteristics determined by the local shock compression ratio (unless the energies are higher than the shock is capable of accelerating particles to, in which case the spectral index is unchanged although the distribution experiences compression). Because of the pre-existing energetic particle population, we focus on event-integrated spectra rather than the evolution of the accelerated spectrum at 1 AU. The former is largely independent of the pre-existing energetic particle population whereas the latter can be contaminated by features of the initial spectrum. The event-integrated spectra will reflect fully the characteristics of the later shock as it propagates to 1 AU.

Verkhoglyadova et al. (2007) find that the shock reaches 1 AU in $\sim$ 50 hours. They model the acceleration and transport of protons and Fe and (CN)O ions, with a charge to mass ratio of 14:56 and 6:16 respectively, in the vicinity of the quasi-parallel shock. As the shock propagates it slows and the maximum energies to which the particle species can be accelerated decreases (Figure 1), and is inversely proportional to the (Q/A) of the ion species. Accelerated particles leak/escape from the shock and propagate to 1 AU and beyond. Figure 8 shows the integrated proton, iron and oxygen spectra at 1 AU. A power law with theoretical limit of $\sim (s+2)/(s-1)/2$ (shown by

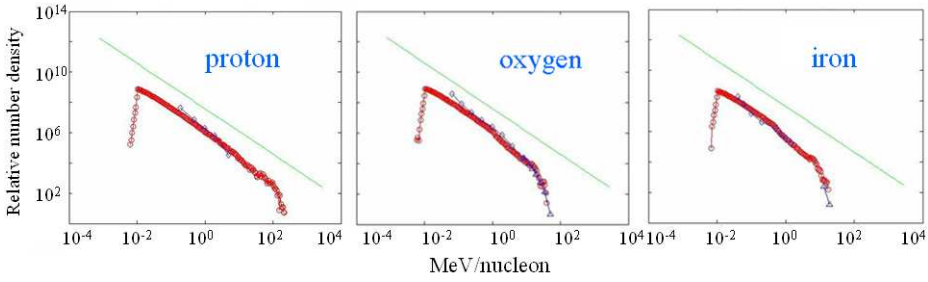

Figure 8. Event integrated proton, iron, and oxygen spectra at 1 AU determined by the PATH model(red circles) and compared to ACE SIS (blue triangles) and ULEIS (blue diamonds) measured spectra. Verkhoglyadova et al. (2007)

the green line) is plotted to guide the eye for $s = 2.3$. Corresponding data taken from ACE measurements are also plotted. We use ULEIS (Mason et al., 1998) and SIS (Stone et al., 1998) particle detectors to estimate the integrated fluxes and spectra. The low-energy part of the spectrum is fitted to ULEIS measurements (shown by diamonds) and the high-energy part is fitted to SIS measurements (shown by triangles). Note that the modelled fluxes are presented in arbitrary units (see Verkhoglyadova et al. (2007) for details).

The spectral shapes are interesting in that they possess a "double power-law" structure with the break in energy ordered approximately by $(Q/A)^2$. Although the underlying diffusive shock acceleration theory predicts only strict power laws at any given time at the shock front, that the event-integrated spectra show a break or roll-over at high energies can be understood by recalling that the event integrated spectrum results from overlaying a series of time-dependent spectra as the shock front propagates to 1 AU. As the maximum particle energy accelerated at the shock front decreases with time and the turbulence responsible for trapping particles in the shock complex weakens at the corresponding wave numbers, the event-integrated spectra no longer receive a contribution at high energies, which results in a "broken power law" or gradual roll-over. That the proton, Fe, and O modelled spectra simultaneously agree so well with observations is remarkable. Finally, we note that by comparing the modelled spectra with observations for different heavy ion species, we can examine the validity of our assumption that this event is quasi-parallel. If acceleration at the shock were dominated by perpendicular diffusion, it would be impossible to fit the modelled spectra

to the observed O and Fe spectra since the maximum energy has a different (Q/A) dependence at a quasi-perpendicular shock, than at a quasi-parallel shock - see equations (6) - (9).

4. Conclusions

For the case of quasi-parallel shocks, we have described a time-dependent model of shock wave propagation in the solar wind, at which particles are accelerated by the diffusive shock acceleration mechanism. The model, called PATH for quasi-parallel shocks, includes local particle injection, Fermi acceleration at the shock, self-consistent excitation of the waves responsible for scattering, particle trapping and escape at the shock complex, and non-diffusive transport in the interplanetary medium, and does remarkably well in describing observed SEP events. This includes spectra, intensity profiles, and particle anisotropies. We model both proton and heavy ion acceleration and transport in gradual events, and can fit simultaneously event integrated spectra for protons, Fe, and O. This allows us to understand the Fe / O ratios, for example. We have begun to model mixed events to explore the consequences of a pre-accelerated particle population (from flares, for example) and have also related this to the timing of flare-CME events. These results are not discussed here (Li and Zank, 2005), nor did we discuss preliminary results for multi-D shocks and particle acceleration.

Secondly, we discussed a basic theory for particle acceleration at highly perpendicular shocks based on the convection of *in situ* solar wind turbulence into the shock. We found that the highest injection energies were needed for quasi-perpendicular shocks rather than for properly perpendicular shocks, making the 90° shock a "singular" example. Unlike the quasi-parallel case, the determination of the perpendicular diffusion coefficient is not based on a resonance condition but on the Nonlinear Guiding Center theory instead. Maximum energies at quasi-perpendicular shocks are smaller than those achieved at quasi-parallel shocks near the sun when self-consistent wave excitation is included. The injection energy threshold is much higher for quasi-perpendicular shocks than for quasi-parallel shocks and we can therefore expect distinctive compositional differences for the two cases. Finally, although not discussed here, observations support the notion that diffusive particle acceleration at shocks can occur in the absence of stimulated wave activity (Zank et al., 2006).

Acknowledgements

The authors acknowledge the partial support of NASA grants NNG04GF83G, NNG05GH38G, NNG05GM62G, a Cluster University of Delaware subcontract BART372159/SG, and NSF grants ATM0317509, and ATM0428880.

References

Axford, W.I., E. Leer, and G. Skadron, Proc. 15th Int. *Cosmic Ray Conf. (Plovdiv), 11*, 132, 1977.

Bell, A.R., The acceleration of cosmic rays in shock fronts. I and II, *Mon. Not. Roy. Astron. Soc.*, 182, 147-156, 443-455, 1978.

Cane, H. V.; Richardson, I. G., Interplanetary coronal mass ejections in the near-Earth solar wind during 1996-2002, J. Geophys. Res., 108,CiteID 1156, DOI 10.1029/2002JA009817, 2003.

Cliver, E. W., and H. V. Cane, Solar Energetic Particles: Acceleration and Transport, AIP Conf. Proc., vol. 516, Am. Inst. of Phys., College Park, Md., (2000).

Cohen, C. M. S., R. A. Mewaldt, R. A. Leske, A. C. Cummings, E. C. Stone, M. E. Wiedenbeck, E. R. Christian, and T. T. von Rosenvinge, New observations of heavy-ion-rich solar particle events from ACE, Geophys. Res. Lett., 26, 2697, (1999).

Desai, M. I., Mason, G. M., Dwyer, J. R., Mazur, J. E., Gold, R. E., Krimigis, S. M., Smith, C. W., Skoug, R. M., Evidence for a Suprathermal Seed Population of Heavy Ions Accelerated by Interplanetary Shocks near 1 AU, Astrophys. J., 588, Issue 2, 1149-1162, 2003.

Drury, L. O., An introduction to the theory of diffusive shock acceleration of energetic particles in tenuous plasmas, Rep. Progr. Phys., 46, 9731027, (1983).

Gordon, B. E.; Lee, A. M.; Mbius, E.; Trattner, K. J., Coupled hydromagnetic wave excitation and ion acceleration at interplanetary traveling shocks and Earth's bow shock revisited, *J. Geophys. Res., 104*, 28,263, 1999.

Heras, A. M., B. Sanahuja, Z. K. Smith, T. Detman, and M. Dryer, The influence of the large-scale interplanetary shock structure on a lowenergy particle event, Astrophys. J., 391, 359 369, (1992).

Heras, A. M., B. Sanahuja, D. Lario, Z. K. Smith, T. Detman, and M. Dryer, 3 Low energy particle events: Modeling the influence of the parent interplanetary shock, Astrophys. J., 445, 497 508, (1995).

Jokipii, J. R., Rate of energy gain and maximum energy in diffusive shock acceleration, Astrophys. J., 313, p842, 1987.

Kahler, S. W., N. R. Sheeley, R. A. Howard, M. J. Koomen, D. J. Michels, R. E. McGuire, T. T. von Rosenvinge, and D. V. Reames, Associations between coronal mass ejections and solar energetic proton events, J. Geophys. Res., 89, 9683 9693, (1984).

Kallenrode, M.-B., and G. Wibberenz, Propagation of particles injected from interplanetary shocks: A black box model and its consequences for acceleration theory and data interpretation, J. Geophys. Res., 102, 22,311 22,334, (1997).

Kallenrode, M.-B., and R. Hatzky, Energetic particle events at traveling interplanetary shocks: Modeling between 20 keV and 500 MeV, Proc. Int. Conf. Cosmic Rays 26th, 6, 324 327, (1999).

Lario, D., B. Sanahuja, and A. M. Heras, Energetic particle events: Efficiency of interplanetary shocks as 50 keV ¡ E ¡ 100 MeV proton accelerators, Astrophys. J., 509, 415 434, (1998).

Lee, M. A., Coupled hydromagnetic wave excitation and ion acceleration at interplanetary traveling shocks *J. Geophys. Res., 88*, p. 6109, 1983.

Leske, R. A., J. R. Cummings, R. A. Mewaldt, E. C. Stone, and T. T. von Rosenvinge, Measurements of the ionic charge states of solar energetic particles using the geomagnetic-field, Astrophys. J., 452, L149L152, (1995).

Li, G., G. P. Zank and W. K. M. Rice, Energetic particle acceleration and Transport at coronal mass ejection drive shocks, *J. Geophys. Res.*, 108(A2), 1082, doi:10.1029/2002JA009666, 2003.

Li, G. and Zank, G. P., Mixed Particle acceleration at CME-driven shocks and Flares, *Geophys. Res. Lett.*, 32, L02101, doi:10.1029/2004GL021250., 2005.

Li, Gang; Zank, G. P.; Rice, W. K. M., Acceleration and transport of heavy ions at coronal mass ejection-driven shocks, *J. Geophys. Res.*, A06104, 2005.

Li, G., G. P. Zank, M. Desai, G. M. Mason, and W. Rice, Particle acceleration and transport at CME-driven shock: A case study, in *Particle Acceleration in Astrophysical Plasmas in Geospace and Beyond*, Geophys. Monogr. Ser., AGU, Washington, D. C., pp. 51-58, 2005.

Luhn, A., B. Klecker, D. Hovestadt, M. Scholer, G. Gloeckler, F. M. Ipavich, C. Y. Fan, and L. A. Fisk, Ionic charge states of N, Ne, Mg, SI and S in solar energetic particle events, Adv. Space Res., 4, 161, (1984).

Luhn, A., B. Klecker, D. Hovestadt, and E. Mobius, The mean ionic charge state of silicon in He-3-rich solar-flares, Astrophys. J., 317, 951955, (1987).

Mason, G. M., J. E. Mazur, M. D. Looper, and R. A. Mewaldt, Charge-state measurements of solar energetic particles observed with SAMPEX, Astrophys. J., 452, 901 911, (1995).

Mason, G. M.; Gold, R. E.; Krimigis, S. M.; Mazur, J. E.; Andrews, G. B.; Daley, K. A.; Dwyer, J. R.; Heuerman, K. F.; James, T. L.; Kennedy, M. J.; Lefevere, T.; Malcolm, H.; Tossman, B.; Walpole, P. H., The Ultra-Low-Energy Isotope Spectrometer (ULEIS) for the ACE spacecraft, Space Science Reviews, v. 86, Issue 1/4, p. 409-448 (1998).

Mason, G. M., et al., Particle acceleration and sources in the November 1997 solar energetic particle event, Geophys. Res. Lett., 26, 141 144, (1999).

Matthaeus, W. H., G. Qin, J. W. Bieber, and G. P. Zank, Nonlinear collisionless perpendicular diffusion of charged particles, Astrophys. J., 590, L53, 2003.

Ng, C. K., and D. V. Reames, Pitch angle diffusion coefficient in an extended quasi-linear theory, Astrophys. J., 453, 890, (1995).

Ng, C. K., D. V. Reames, and A. J. Tylka, Effect of proton-amplified waves on the evolution of solar energetic particle composition in gradual events, Geophys. Res. Lett., 26, 2145 2148, (1999).

Ng, C. K., D. V. Reames, and A. J. Tylka, Modeling shockaccelerated solar energetic particles coupled to interplanetary Alfven waves, Astrophys. J., 591, 461485, (2003).

Oetliker, M., B. Klecker, D. Hovestadt, G. M. Mason, J. E. Mazur, R. A. Leske, R. A. Mewaldt, J. B. Blake, and M. D. Looper, The ionic charge of solar energetic particles with energies of 0.3 70 MeV per nucleon, Astrophys. J., 477, 495 501, (1997).

Rice, W.K.M., Zank, G.P. and Li, G., Particle acceleration at coronal mass ejection driven shocks: for arbitrary shock strength. *J. Geophys. Res., 108*, 1369 doi:10.1029/2002JA009756, 2003.

Ruffolo, D., Effect of adiabatic deceleration on the focused transport of solar cosmic rays, Astrophys. J., 442, 861 874, (1995).

Stone, E. C.; Cohen, C. M. S.; Cook, W. R.; Cummings, A. C.; Gauld, B.; Kecman, B.; Leske, R. A.; Mewaldt, R. A.; Thayer, M. R.; Dougherty, B. L.; Grumm, R. L.; Milliken, B. D.; Radocinski, R. G.; Wiedenbeck, M. E.; Christian, E. R.; Shuman, S.; von Rosenvinge, T. T., The Solar Isotope Spectrometer for the Advanced Composition Explorer, Space Science Reviews, v. 86, Issue 1/4, p. 357-408, 1998.

Tylka, A. J., P. R. Boberg, J. H. Adams, L. P. Beahm, W. F. Dietrich, and T. Kleis, The mean ionic charge state of solar energetic Fe ions above 200 MeV per nucleon, Astrophys. J., 444, L109L113, (1995).

Tylka, A. J., Cohen, C. M. S., Dietrich, W. F., Lee, M. A., Maclennan, C. G., Mewaldt, R. A., Ng, C. K., Reames, D. V., Shock Geometry, Seed Populations, and the Origin of Variable Elemental Composition at High Energies in Large Gradual Solar Particle Events, Astrophys. J., 625, Issue 1, 474-495, 2005.

van Nes, P., R. Reinhard, T.R. Sanderson, K.-P. Wenzel, and R.D. Zwickl, The energy spectrum of 35- to 1600-keV protons associated with interplanetary shocks, *J. Geophys. Res., 89,* 2122, 1984

Verkhoglyadova, O.P., Li, G., Zank, G.P., and Q. Hu, Gradual SEP Event of September 29, 2001 and comparison with ACE measurements, manuscript in preparation, 2007.

Zank, G. P., H. L. Pauls, I. H. Cairns, and G. M. Webb, Interstellar pick-up ions and perpendicular shocks: Implications for the termination shock and interplanetary shocks, J. Geophys. Res., 101, 457, 1996.

Zank, G.P., W.H. Matthaeus, J.W. Bieber, and H. Moraal, The radial and latitudinal dependence of the cosmic ray diffusion tensor in the heliosphere, *J. Geophys. Res. (Space), 103*, 2085-2097 (1998).

Zank, G.P., W.K.M. Rice, and Wu, C.C., Particle acceleration and coronal mass ejection drive shocks: A theoretical model, *J. Geophys. Res. (Space), 105*, 25079-25095, 2000.

Zank, G. P., G. Li, V. Florinski, W. H. Matthaeus, G. M. Webb, and J. A. le Roux, Perpendicular diffusion coefficient for charged particles of arbitrary energy, J. Geophys. Res., 109, A04107, doi:10.1029/2003JA010301, 2004.

Zank, G.P., Gang Li, V. Florinski, Qiang Hu, D. Lario, and C.W. Smith, Particle acceleration at perpendicular shock waves: Model and observations, 1, *J. Geophys. Res.*, **1**, 1., Issue A6, CiteID A06108 (2006).